

Article

Flexural Behavior of the Composite Girder of a Prestressed Segmental UHPC Channel and a Reinforced Conventional Concrete Deck

Yicong Chen ¹, Jialiang Zhou ^{1,*}, Baochun Chen ¹, Jiazhan Su ¹ and Camillo Nuti ² ¹ College of Civil Engineering, Fuzhou University, Fuzhou 350108, China² Department of Architecture, Roma Tre University, 00153 Rome, Italy

* Correspondence: m170510014@fzu.edu.cn

Abstract: The present study was conducted to clarify the flexural behaviors of the Composite Girders of a Prestressed Segmental Ultra-High-Performance Concrete (UHPC) Channel and a Reinforced Conventional Concrete Deck (PSUC-RCCD). The girders can be used as bridge superstructures with the advantages of structural efficiency, cost-effectiveness, and easy construction. A total of five specimens were tested. Three of them were PSUC-RCCD specimens, including two semi-segmental girders (the channel beams were composed of five segments with dry-joints) and one integral girder (the channel beams were integral ones without dry-joints). The two other specimens were P-UHPC girders composed of PSUC and UHPC deck slabs; one was semi-segmental and the other was integral. The flexural behaviors of the specimens were investigated, including the load-displacement curves, crack distribution, cracking moments, and ultimate flexural capacity. The study compared the influence of the segment number and deck material on the flexural behaviors of semi-segmental girders and introduced and validated methods for calculating the cracking moment and flexural capacity of both semi-segmental and integral sections in PSUC-RCCD and P-UHPC girders. The results show that the entire loading process of all the specimens can be classified into the elastic phase, the cracks development phase, and the failure phase. Compared to the integral girders, the number of segments has little effect on the flexural behavior of the semi-segmental girders, but it has a significant effect on the cracking moments. The cracking moments of the semi-segmental girders is only 0.58~0.60 of the integral girders. Reducing the strength of the deck slab by changing the material from UHPC to CC does not significantly affect their flexural behaviors. Based on the test results, this work proposes a method for predicting the cracking moment and flexural capacity of the semi-segmental girders, the results of which fit well with the test results, and it is applicable in the structural design of such members.

Keywords: UHPC; composite girder; segmental channel; conventional concrete (CC); flexural test; calculations



Citation: Chen, Y.; Zhou, J.; Chen, B.; Su, J.; Nuti, C. Flexural Behavior of the Composite Girder of a Prestressed Segmental UHPC Channel and a Reinforced Conventional Concrete Deck. *Buildings* **2023**, *13*, 3132. <https://doi.org/10.3390/buildings13123132>

Academic Editor: Ramadhansyah Putra Jaya

Received: 13 November 2023

Revised: 12 December 2023

Accepted: 16 December 2023

Published: 18 December 2023



Copyright: © 2023 by the authors. Licensee MDPI, Basel, Switzerland. This article is an open access article distributed under the terms and conditions of the Creative Commons Attribution (CC BY) license (<https://creativecommons.org/licenses/by/4.0/>).

1. Introduction

Research on Ultra-High-Performance Concrete (UHPC) is a hot topic in the realm of civil engineering in recent decades and has achieved significant progress in its material science and technology [1–4]. Although some progress has been made in the application and research of UHPC, UHPC is still a new material at present. Researchers are still exploring the structure and material properties of UHPC. For the material properties of UHPC, for example, Mostafa et al. [5] investigated the influence of four different nanomaterials on UHPC, showed that the compressive strength is significantly improved, and reduced the value of absorption by adding the nano-particles.

At the same time, its commercial use has been developing rapidly in civil engineering thanks to its superior mechanical traits and durability, especially in bridge construction [6,7].

In China, UHPC becomes desperately needed in bridge engineering because it faces increasingly serious challenges including energy saving, CO₂ reduction, and the pollution of air after about four decades of large-scale infrastructure construction with numerous conventional concrete (CC) structures [8]. To reduce the plate self-weight, UHPC was first applied in bridge engineering in China as the void plates in the dividing strip of the Shijingshan cable-stayed bridge in Beijing in 2003 [9]. Then UHPC cover plates for cable channels and sidewalk slabs have been widely adopted in high-speed railways ever since about 2005 [10]. The first two railway UHPC bridges in China are simply supported by precast prestressed T-shape UHPC girders, one located in the Qian-Cao railway line with a span of 20 m built in 2006, and the other one in the Ji-gang railway covering a particular span of 32 m, built in 2008 [11]. Since 2011, the UHPC thin layer (about 45 mm to 60 mm depth) has been used in more than 30 bridges to stiffen the orthotropic steel deck to prevent the fatigue of the steel structure as well as the early damage of the asphalt overlay [12]. The first UHPC highway bridge built in 2015 features four continuously connected spans of 30 m each, which cross over the expressway from Beijing to Zhuhai at K34 + 690 [13]. The first pedestrian bridge is a landscape bridge at Fuzhou University campus, which is an arch bridge, built in 2015 [14]. A significant application of UHPC in Chinese bridge structures in the last years may be the major girder of the No. 5 Nanjing Yangtze River Bridge cable-stayed bridge completed in 2020, which consists of a steel girder-UHPC deck slab with two main spans of 600 m [15].

China is still in the process of constructing large-scale infrastructure systems, so it is essential to have more innovative UHPC bridge structures with more benefits from this advanced material to promote its application. The composite girder studied in this paper is one of these UHPC bridge structures, which consists of a Prestressed Segmental UHPC Channel and a Reinforced Conventional Concrete Deck (Abbreviated as PSUC-RCCD). In construction, the UHPC channel segments of a beam are fabricated, with each segment matched cast in factory and then delivered to site (a); they are assembled and prestressed together by prestressing bars to be a channel beam, which is then erected on the design position; after all the UHPC channel beams have been erected, the RCCD slab is cast in situ to form the final bearing structure, i.e., the PSUC-RCCD composite girders. The benefits of such a structure include but are not limited to:

- (1) Precasting the UHPC segments in a factory allows for steam curing and storage for some time, which can complete most of the shrinkage, resulting in a less negative effect of shrinkage.
- (2) Each channel segment is not heavy and can be transported to the site and erected to the design position by conventional lorry and hoisting equipment. This can make the transportation process easier and more cost-effective, as shown in Figure 1a.
- (3) The segments are cast by matching each other and are assembled together by post-tensioning without wet joints in the site, which can make the construction simple and faster, as shown in Figure 1b.
- (4) UHPC has ultra-high compressive strength but cannot play the whole role in the flange with compressive stresses generally [13]; instead, conventional concrete (CC) with a lower compressive strength can be more efficiently used. Moreover, the CC cast in situ for the whole deck slab can improve the integrity of the girder, as shown in Figure 1c.

Overall, the benefits of using PSUC-RCCD composite girders include improved durability, efficient load-bearing, easy transportation and construction, and an improved integrity of the girder.

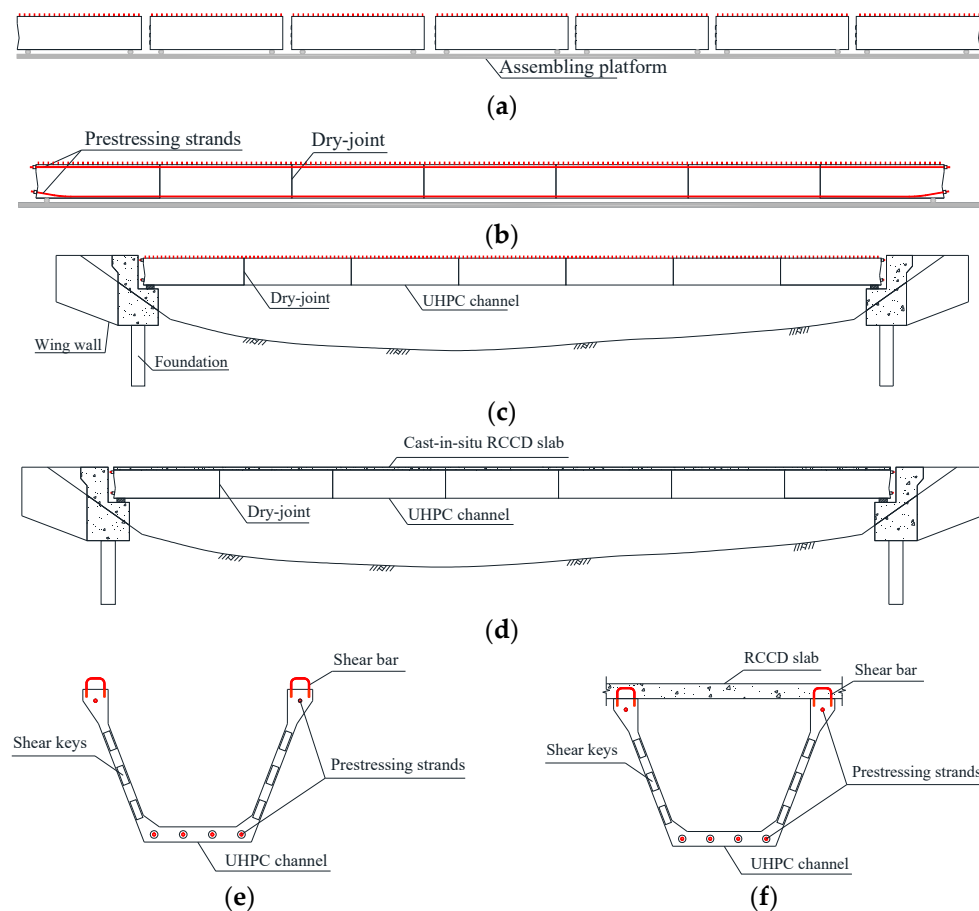


Figure 1. PSUC-RCCD Composite Bridge Construction Process. (a) Precast UHPC segment (section 1-1); (b) Assembled into a UHPC channel beam (section 1-1); (c) Erection of the UHPC channel beam (section 1-1); (d) Cast in situ for the whole deck slab (section 2-2); (e) section 1-1; (f) section 2-2.

Compared to several bridge structures, they have the following advantages.

- (1) For full-section segmental UHPC box girders. The integrity and seismic performance of the box girder is improved by further connecting the segmental U-shaped beams through the cast-in-place concrete deck. At the same time, when the bridge fails, the segmental beams will not directly fall off completely due to the failure of the prestressing cables, which strengthens the safety of the structure;
- (2) For UHPC-RC box girders. The prefabrication of UHPC girder segments in the factory is more convenient for UHPC to carry out high-temperature and pressurized maintenance to ensure the quality of the girder segments. On-site construction avoids the erection of supports, reduces the interference with the lower traffic and construction costs, and significantly improves the construction efficiency. When the segment is damaged, the bridge can be repaired by replacing the girder segments, which is conducive to the sustainable development of the bridge;
- (3) For steel-concrete composite structures. The amount of on-site welding work and the necessity of the anticorrosive coating of steel beams are eliminated. At the same time, it avoids the problems of different temperature gradients and an excessive stiffness difference between the steel beams and concrete slabs caused by changes in the ambient temperature, and it has obvious advantages in terms of the whole life cycle cost and durability. In addition, the UHPC girder has greater stiffness and less deformation during construction, and the combined PSUC-RCCD girder has greater stiffness.

Therefore, structures with so many advantages are urgently needed to be promoted and applied. However, there are still some questions about this type of structure, such as whether the integral casting of RCCD slabs helps to keep the integrity of the segmental beams and whether the top slab will not reduce the strength, for which we need to carry out an experimental study to provide a basis for the popularization of the new structure.

Though few studies on PSUC-RCCD composite girders have been carried out, and some bridges using this type of girder have been built in Malaysia [16,17], questions remain about their design and behavior under flexure. One of the main concerns is its flexural behavior. As is well known, UHPC is generally reinforced by steel fibers, has a higher tensile strength, and can exhibit a good post-cracking capacity owing to the crack-bridging capacity of steel fiber reinforcement [5,18], while the steel fibers in the segmental UHPC channel are dispersed by the dry-joints, which must influence the flexural behavior. However, research on this is scarce. Makhbal et al. [19] carried out a test on a PSUC-reinforced high-performance concrete deck slab composite girder. The final test results indicated that the composite girder possessed a flexural capacity higher than the design required. However, the test was terminated before it failed, so the failure mode and the maximum capacity were not discovered. Lee et al. [20] drew a comparison regarding the flexural performance of segmental U-beams with or without a deck slab. It was pointed out that the composite U-beam with a high-strength concrete slab could improve the ductility and flexural capacity. The study of PSUC-RCCD composite girders is still relatively limited compared to that of the flexural behavior of ordinary reinforced concrete girders, which severely limits the popularization of these girders.

The authors [21] have also completed pre-experiments on the flexural behavior of two PSUC-RCCD girders by conducting FEM and parametric analysis. It was found that the ultimate loads of the semi-segmental and integral girders were rather close. However, due to the lower amount of test data of the specimens, some of the conclusions are still not well convinced by extensive finite element simulations and analyses. Therefore, further experimental studies on the bending properties of PSUC-RCCD girders should be necessarily conducted. Thus, building on the pre-experiment results of the simulation and parametric analysis, five PSUC-RCCD girders were designed in this paper for the bending experiments. The research program in this study aimed to clarify the flexural behavior shared by PSUC-RCCD composite girders, thereby contributing to the development of better design practices for this type of girder.

2. Experimental Procedures

2.1. Specimens

2.1.1. Parameters

Two parameters were considered in the design of the specimens. One was the segment number and the other was the material of the deck slabs. The main specimen parameters are listed in the following Table 1.

Table 1. Main specimen parameters.

Girder Notations	Segment Number	Deck Slab Material
PSUC-RCCD-5(1)	5	CC
PSUC-RCCD-5(2)	5	CC
PSUC-RCCD-1	1	CC
P-UHPC-5	5	UHPC
P-UHPC-1	1	UHPC

Three specimens were PSUC-RCCD composite girders. Two of them were semi-segmental girders, in which the UHPC channel beams were made by five precast segments, connected by dry-joints without shear keys on the interfaces. These two specimens that have exactly the same parameters were the basic specimens in this study and were named

as PSUC-RCCD-5(1) and PSUC-RCCD-5(2), where “5” represents the segment number of the specimen. The rest specimen was an integral girder, in which the UHPC channel beam was an integral one, i.e., the segment number was 1. This specimen was called PSUC-RCCD-1.

In the other two specimens, both the channel beams and the deck slabs were made by UHPC, so they were prestressed UHPC (P-UHPC) girders. They were called P-UHPC-5 and P-UHPC-1, respectively. The former one was a semi-segmental girder with five segments for its channel beam, and the other one was an integral girder with only one segment for its channel beam.

2.1.2. Size and Reinforcement

Five girders were fabricated and tested, all being 3800 mm in length, covering an effective span of 3600 mm. Those general cross-sections of girders were a trapezoidal box featuring a depth of 380 mm, a width of 260 mm, and 50 mm as well as 70 mm thicknesses of the webs and flanges, respectively, while the end cross-section was solid with a length of 200 mm at each side, as shown in Figure 2.

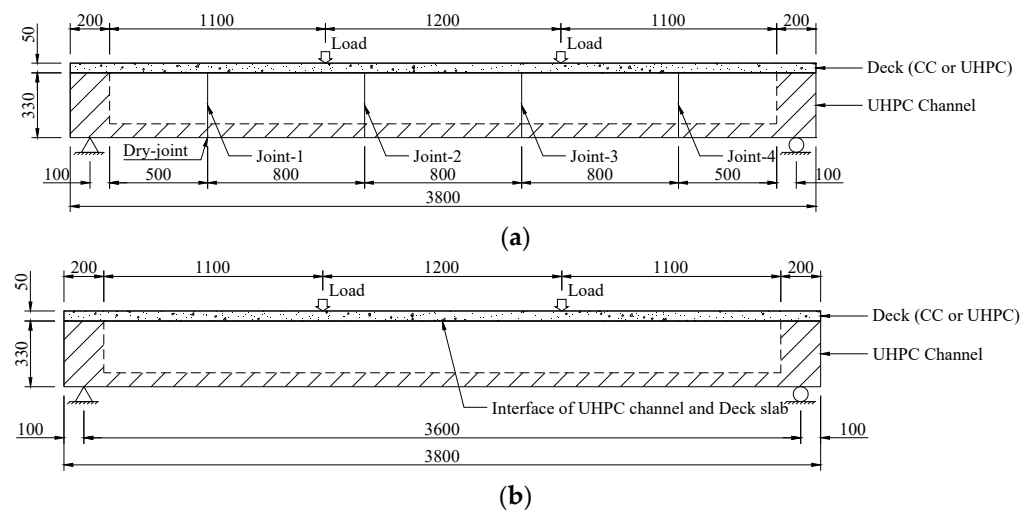


Figure 2. Specimen elevation (unit: mm). (a) PSUC-RCCD-5(1), PSUC-RCCD-5(2) and P-UHPC-5; (b) PSUC-RCCD-1 and P-UHPC-1.

The UHPC channel beam had no longitudinal reinforcement or stirrup within the pure bending zone (1200 mm). A girder was prestressed by 15.2 mm prestressing strands at the bottom flange, each with a mean effective tensile stress of 152.5 kN. The other two strands were arranged at the top of the two webs (one for each), each with a mean effective tensile stress of 20 kN to prevent the top joint from opening when the bottom slab was prestressed. The channel beam was linked to the deck slabs using shear bars featuring a diameter of 6 mm, as shown in Figure 3.

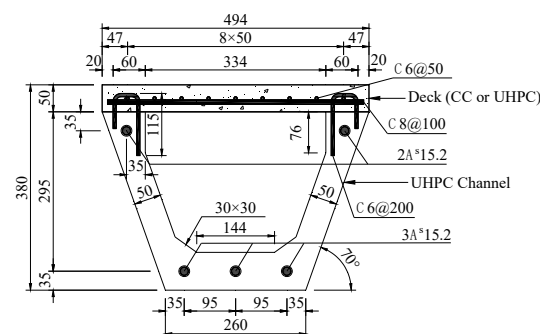


Figure 3. Reinforcement arrangement (unit: mm).

Though there were shear keys in the actual project [16,22,23], they were small in dimension and there were generally only three in each web section (see Figure 1c). However, no shear key was applied in this study due to the fact that the web was too thin to have one; moreover, it was estimated by the pre-analysis of the experimental program that the test specimens would not fail by shear failure.

2.1.3. Fabrication

The UHPC segments were steam-cured for 3 days at a rather high temperature (about 90 °C) and cured at a normal temperature for one month. For the specimens PSUC-RCCD-5(1), PSUC-RCCD-5(2) and P-UHPC-5, the segmentation of the formwork of the integral beam by means of diaphragms and the subsequent casting of the UHPC segments ensured a good fit between the UHPC segments. The channel segments were connected by dry-joints and post-tensioned to form an integral girder. The formwork and reinforcement were supported on the pre-fabricated UHPC channel girders; CC or UHPC was poured and a second maintenance was carried out. The fabrication of PUSC-RCCD girders and P-UHPC girders was completed.

2.2. Material Properties

Tables 2 and 3 provide the composition details of the UHPC and CC mixtures, respectively. In the UHPC mix, a straight steel fiber (SSF) was incorporated, contributing to a 2% fiber volume fraction (length/diameter ratio of 65).

Table 2. Mix proportion of UHPC.

Cement	Silica Fume	Quartz Sand			Quartz Powder	Superplasticizer	Water
		Coarse 40–70	Medium 20–40	Fine 10–20			
1.00	0.30	0.14	0.41	0.53	0.09	0.02	0.23

Table 3. Mix proportion of CC.

Cement	Flyash	Gravel	River Sand	Superplasticizer	Water
1.00	0.15	2.23	1.43	0.02	0.32

The cement is Portland cement (P.O 42.5), which was used as the binder; the silica fume was used as a filler material, which has a specific surface area of $1.89 \times 10^4 \text{ m}^2 \cdot \text{kg}^{-1}$ and an SiO_2 content of more than 90%. The particle sizes of the quartz sand were less than 0.6 mm, and its mesh size and percentage are shown in Table 2. The polycarboxylate superplasticizer is a CX-8 type with a water reduction of more than 25%, which provides good workability at a low water–binder ratio.

The flyash was used as a filler material, which has a specific surface area of $400 \text{ m}^2 \cdot \text{kg}^{-1}$ and an SiO_2 content of more than 65%. The particle sizes of the gravel and river sand were less than 5 mm and 0.6 mm, respectively. Other material parameters are the same as those mentioned in the UHPC.

The material properties of UHPC were obtained by coupon tests according to the code [24]. This involved testing $100 \times 100 \times 300$ mm prisms to obtain the compressive strength and modulus of elasticity. Additionally, axial tensile strength data were obtained from tests conducted on dog bone specimens [25].

The material properties of CC were investigated by conducting coupon tests in accordance with the code [26]. Its compressive strength and modulus of elasticity were explored by testing the $150 \times 150 \times 450$ mm prisms. Due to the test conditions, the splitting tensile strength of CC was acquired based on the tests conducted on the $100 \times 100 \times 100$ mm cubes.

The final test results for UHPC and CC are illustrated in Table 4.

Table 4. Material properties of UHPC and CC.

Material	f_c /MPa	f_{t0} /MPa	ε_{t0} / $\mu\varepsilon$	f_t /MPa	ε_t / $\mu\varepsilon$	E_c /GPa
UHPC	134.2	5.7	131.2	8.7	2736.4	44.9
CC	53.1	-	-	3.8	-	38.4

f_c is the compressive strength, f_{t0} is the tensile cracking strength, ε_{t0} is the tensile cracking strain, f_t is the tensile strength, ε_t is the tensile strain, and E_c is the elastic modulus.

The characteristics of the utilized steel were established using coupon tests following the guidelines outlined in [27]. The final experimental results for both the prestressing strand and steel reinforcement are detailed in Table 5. The nominal yield strength of the prestressing strand was defined as the stress with a residual strain of 0.002.

d is the diameter, A_p is the cross-sectional area of the steel, f_p is the yield strength, ε_{pt} is the yield strain, f_{pu} is the ultimate strength, ε_{pu} is the ultimate strain, and E_p is the elastic modulus of the steel.

Table 5. Steel properties.

Material	d /mm	A_p /mm ²	f_p /MPa	ε_{pt} / $\mu\varepsilon$	f_{pu} /MPa	ε_{pu} / $\mu\varepsilon$	E_p /GPa
Prestressing strand	15.2	139.0	1521	0.0108	1887	0.0639	1.94×10^5
Steel reinforcement	6.0	28.3	400	0.0020	570	0.0260	2.02×10^5

2.3. Test Setup, Instrumentation, and Loading Protocol

2.3.1. Test Setup and Instrumentation

The deflection at five specified positions along the girder span was monitored by installing displacement transducers beneath the girder, as illustrated in Figure 4 (T1~T5). Concrete strain gauges (S1 through S7) were strategically placed at the joint interface between the beam and slab to measure coordinated deformations. In addition, concrete strain gauges (W1~W3) were positioned on the mid-span web, combined with strain gauges S1, to measure the concrete strain at various depths within the test girder. A prestress transducer was affixed to the prestressed steel strand to record transducer strain values during the loading process and to determine the increment of prestress. Data from the displacement transducers, strain gauges, and prestress transducer were all captured and recorded using the DH3816 static strain testing system. The ZBL-F101 crack width meter was utilized to measure the width of cracks in the girders.

2.3.2. Loading Protocol

The specimens were set up with a simple support on one end and a hinge support on the other end, with loading applied at two symmetrical points (as depicted in Figure 4). Meanwhile, the present test also adopted a force-controlled loading protocol. The load was enhanced up to the girder failure monotonically, with each of the specimens pre-loaded with 30 kN before the tests for eliminating the inelastic strain and ensuring the smooth operation of the instrumentation system. Before and after the occurrence of cracks, graded loading with loading intervals of 10 kN and 5 kN was respectively adopted. Between stages, the loading was halted for about 10 min to record the cracks. The test ended in the case of the specimen failing to maintain the load.

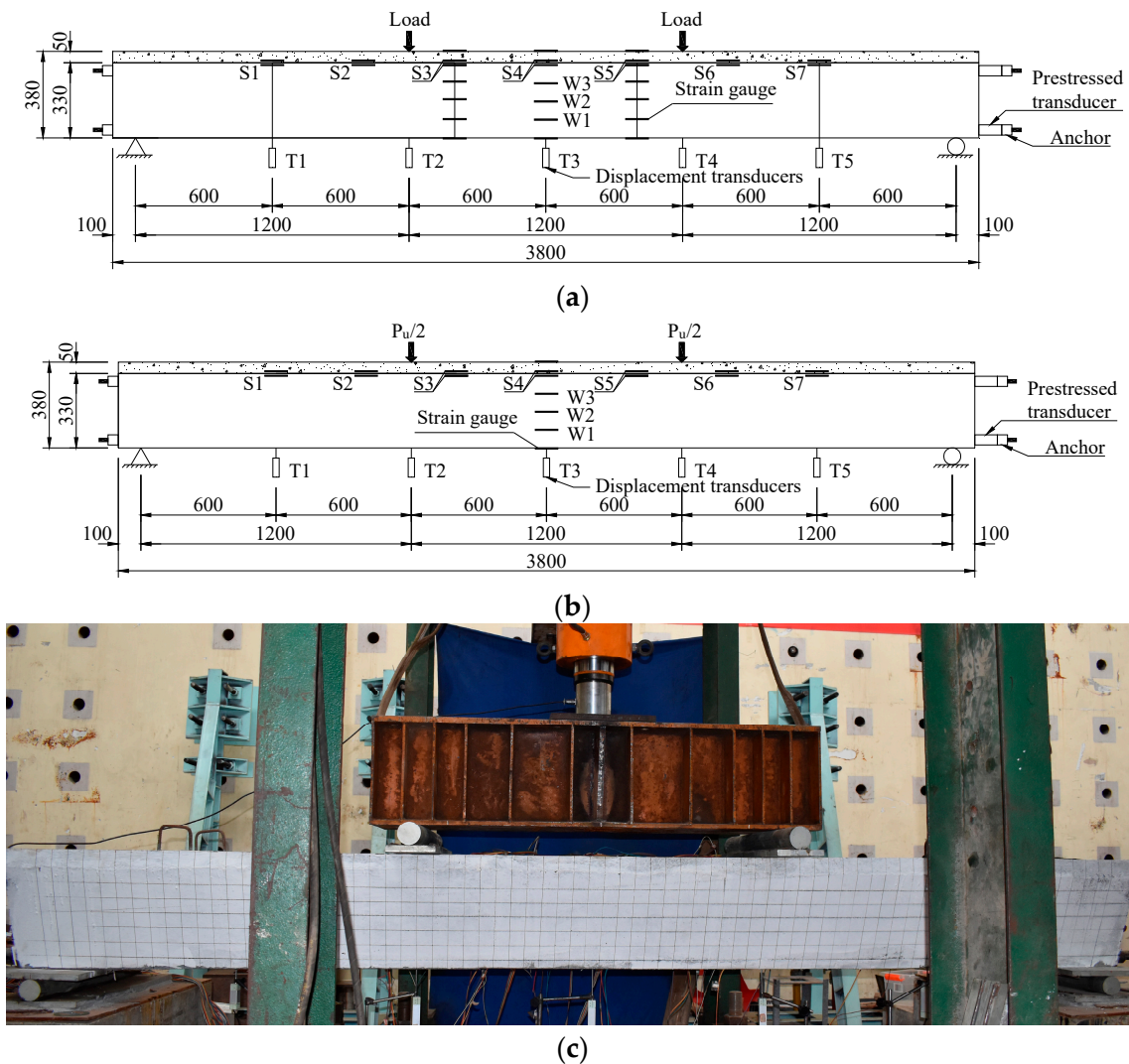


Figure 4. Specimen elevation (unit: mm). (a) PSUC-RCCD-5(1), PSUC-RCCD-5(2) and P-UHPC-5; (b) PSUC-RCCD-1 and P-UHPC-1; (c) Test set-up.

3. Experimental Results

3.1. Behaviors of the Basic Specimens

3.1.1. Basic Behaviors

The loading history and failure mode of all five specimens are similar (as shown in Figure 5a). The load–deflection curves of the specimens initially developed linearly, and we refer to this stage as the elastic phase. After the specimens cracked, the curves became significantly nonlinear, and the vertical cracks continued to develop upward, which we call the crack developing phase. When the prestressing strand reaches the nominal yield strength, the growth rate of deflection and the crack width increase, and finally, the deck slab crashes; we call this stage the failure phase. Therefore, only the behaviors of the two basic specimens, PSUC-RCCD-5(1) and PSUC-RCCD-5(2), are described in detail in this section. For the other specimens, we will describe them by comparison in the subsequent sections.

As presented in Figure 5b, the load–deflection curves at the mid-span of the two basic specimens almost coincide, indicating they had similar behaviors. According to the curves, their loading process can be categorized into three different phases of the elastic phase, the crack developing phase, and the failure phase. Therefore, PSUC-RCCD-5(1) is used to describe the following. The points A~C of the two curves are the same only point D is

different, therefore, for points A~C, there is no need for color differentiation, and for point D, red indicates PSUC-RCCD-5(1) and black indicates PSUC-RCCD-5(2).

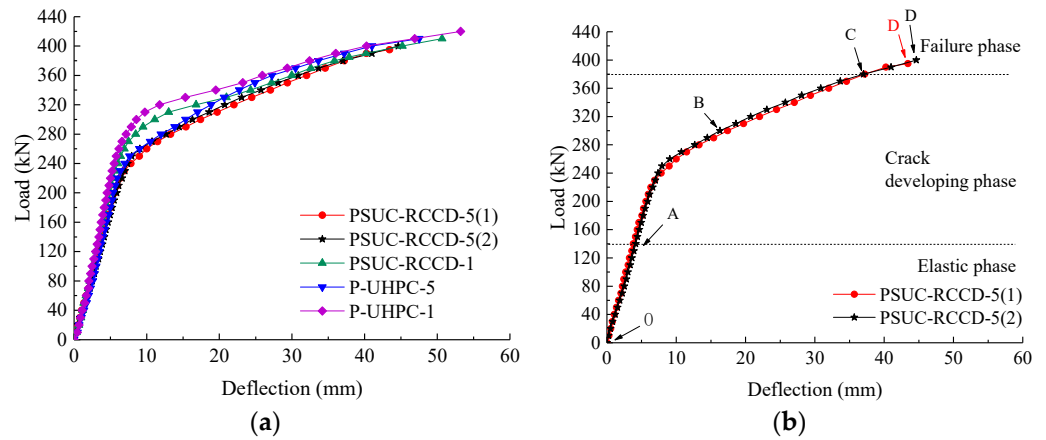


Figure 5. Load-deflection relationships of girders. (a) All girders; (b) basic girders.

As indicated in Figure 6 (where, after the load reached 300 kN, the values could not be obtained due to the cracking of P-UHPC-1 through the concrete strain gauges), the concrete strains of PSUC-RCCD-5(1) and PSUC-RCCD-5(2) were distributed along the beam section linearly before cracking, satisfying the assumption of the plane section. After cracking, the neutralization axis moved up obviously, and the test girder still tallied with the assumption of the plane section. On the other hand, it can be seen that the channel and slab have favorable co-deformation.

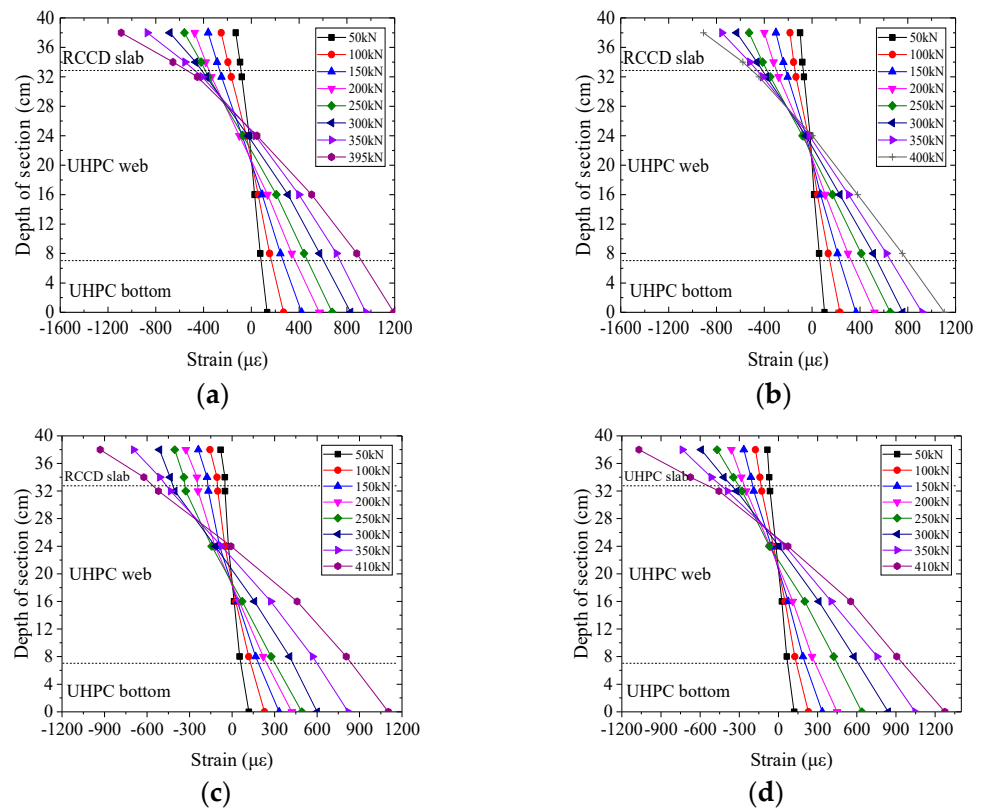


Figure 6. Cont.

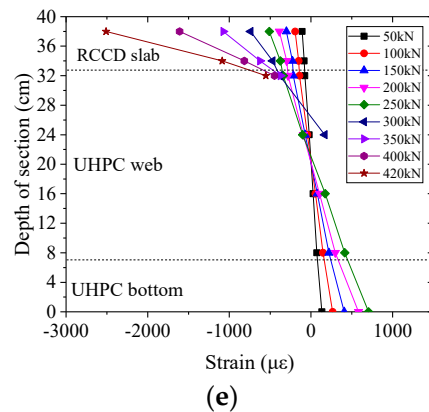


Figure 6. Concrete strain distribution along the depth of the girder. (a) PSUC-RCCD-5(1); (b) PSUC-RCCD-5(2); (c) PSUC-RCCD-1; (d) P-UHPC-5; (e) P-UHPC-1.

3.1.2. Three Phases in the Whole Loading Process

Elastic Phase

In the elastic phase (Curve OA), the mid-span deflection of the specimen increased linearly with the increase in the load. When the load reached 35% P_u (140 kN; P_u denotes the ultimate load), the specimen cracked and the deflection was 9% W_u (3.8 mm; W_u is the ultimate deflection). The elastic phase ended when the first crack was observed in the dry-joint-2 featuring a width of 0.05 mm and a length of 9 cm.

Crack Development Phase I

The first crack in the dry-joint-2 is the start point of the second phase (AB). With the load, both the width and the length of this first crack were developed. When the load reached 51% P_u (200 kN), a second flexural (vertical) crack appeared at joint-3. The corresponding deflection at the mid-span was 13% W_u (5.6 mm). And then the curve showed apparent nonlinearity and the structural stiffness decreased continuously.

At a load of 170 kN, which corresponds to 43% P_u , a horizontal crack measuring 0.05 mm in width and extending to a length of 4.8 cm materialized at the top of joint-2, precisely along the interface connecting the channel-deck. It is essential to note that, at this juncture, no flexural crack had yet developed on the deck slab of the UHPC channel. Subsequently, when the specimen was subjected to a load of 210 kN, equivalent to 53% P_u , a second horizontal crack, with the same dimensions (0.05 mm wide and 9 cm long), appeared at the interface of joint-3.

When the applied load reached 84% of its maximum capacity, equivalent to 330 kN, the first crack extended to the deck level at point B. At this juncture, the crack width expanded to 3.8 mm. Simultaneously, the specimen exhibited a deflection of 56% of its maximum capacity, which amounted to 24.5 mm.

Crack Development Phase II

After point B, no significant change was found in the stiffness of the specimen until point C. At 91% P_u (360 kN), a second crack also reached the deck. The crack width was enlarged to 6.0 mm. The deflection of the specimen was 73% W_u (32.0 mm).

When the load reached 96% P_u (380 kN, point C), in the specimen, the stress increase of the prestressing strands was 446.4 MPa. The total stresses in prestressing strands reached 1536.4 MPa, exceeding the yield strength of 1520 MPa. At this time, the deflections of the specimen were 37.2 mm. The maximum crack width of the specimen reached 9 mm.

Failure Phase

After yielding the prestressing strands, the specimens came to the failure phase (Curve CD). The deflection growth rate of the specimen increased, the width of flexural cracks

increased faster, flexural cracks were further developed in joint-2 toward the top-side of the RCCD slab, and the horizontal cracks in joint-2 and joint-3 started to be connected.

At point D, the RCCD slab at the top of joint-2 in the girders crashed, and the girders failed by flexural failure. The load at Point D is taken as the test ultimate load P_u in this study, it is 395 kN and 400 kN for basic girders, respectively.

The ultimate deflection W_u at the mid-span of the basic girder was 43.4 mm and 45.6 mm, respectively. They are about 1/80 of the effective spans of the specimens. And the stresses in the prestressing strands reached 1585 MPa and 1599 MPa, respectively.

The post-failure crack patterns of both specimens are depicted in Figure 7, with load values in parentheses (kN) and crack widths indicated outside the parentheses (mm). The maximum crack width of PSUC-RCCD-5(1) and PSUC-RCCD-5(2) at failure was 12 mm and 13 mm, respectively. As can be seen in Figure 7, there were no flexural cracks within each segment; the cracks at joint-2 and joint-3 developed similarly, while joint-1 and joint-4 remained closed.

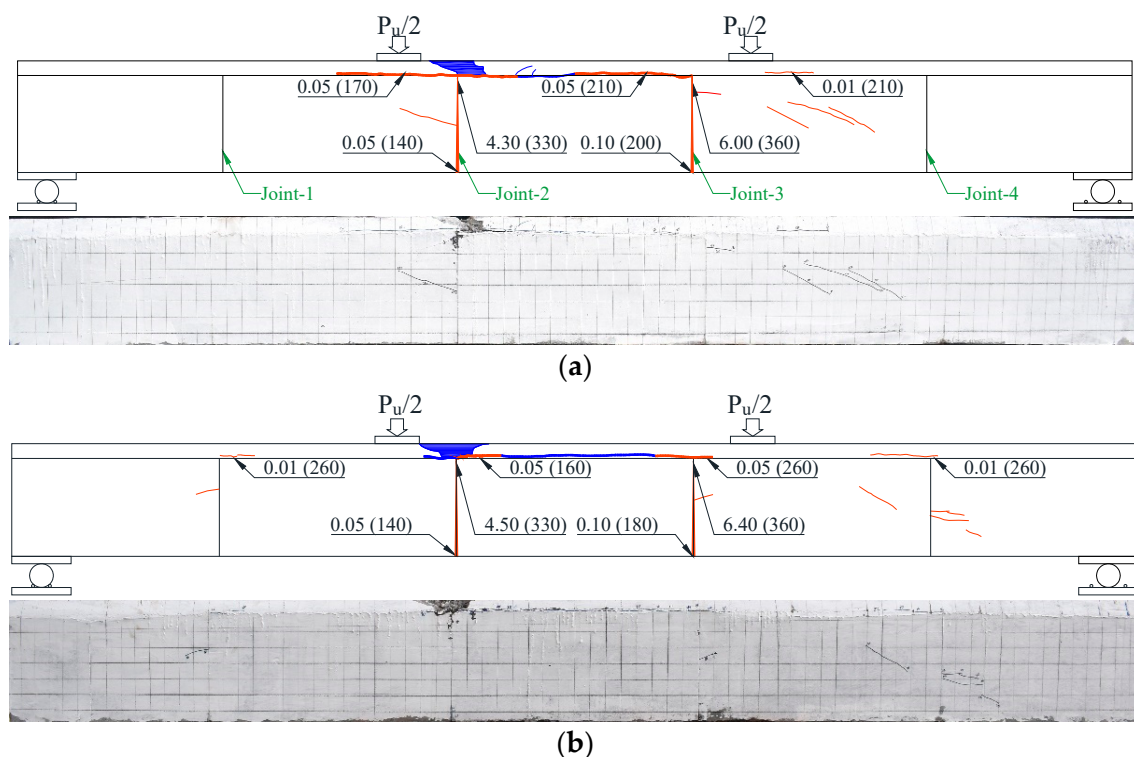


Figure 7. Schematic diagram of the PSUC-RCCD-5(1) and PSUC-RCCD-5(2) specimens in an ultimate load. (a) PSUC-RCCD-5(1) crack pattern in a 395 kN load; (b) PSUC-RCCD-5(2) crack pattern in a 400 kN load.

In addition, the horizontal cracks in segment-2 and segment-3 were interconnected when the girder failed, and no horizontal cracks appeared at the two end segments (segment-1 and segment-4). This means that the RCCD slab and the UHPC channel beam can work as an integral member, and Figure 6 shows that the specimen follows the assumption of the plane section remaining a plane after deformation.

3.2. Parametric Analysis

In this section, the flexural behaviors of all five specimens were analyzed using two parameters. As listed in Table 6, for the parameter of the segment number, PSUC-RCCD-5(1) (or PSUC-RCCD-5(2)) and PSUC-RCCD-1 were bracketed as Group 1-1 (RCCD slab), and P-UHPC-5 and P-UHPC-1 were bracketed as Group 1-2 (UHPC slab); for the parameter of the deck material, PSUC-RCCD-5(1) (or PSUC-RCCD-5(2)) and P-UHPC-5 were bracketed

as Group 2-1 (five segments), and PSUC-RCCD-1 and P-UHPC-1 were bracketed as Group 2-2 (one segment).

Table 6. Groups of the specimens.

Group	Parameters: Segment Number	Group	Parameters: Deck Material
Group 1-1	PSUC-RCCD-5(1) PSUC-RCCD-1	Group 2-1	PSUC-RCCD-5(1) P-UHPC-5
Group 1-2	P-UHPC-5 P-UHPC-1	Group 2-2	PSUC-RCCD-1 P-UHPC-1

In addition, the PSUC-RCCD-5(1), PSUC-RCCD-5(2), and P-UHPC-5 were referred to as semi-segmental girders. The PSUC-RCCD-1 and P-UHPC-1 were referred to as integral girders.

3.2.1. Segment Number

Load-Deflection Curve of Group 1-1 and Group 1-2

In Figure 8, the comparison curves of the load-deflection of the two groups are similar; only the comparison curve of Group 1-1 is described here.

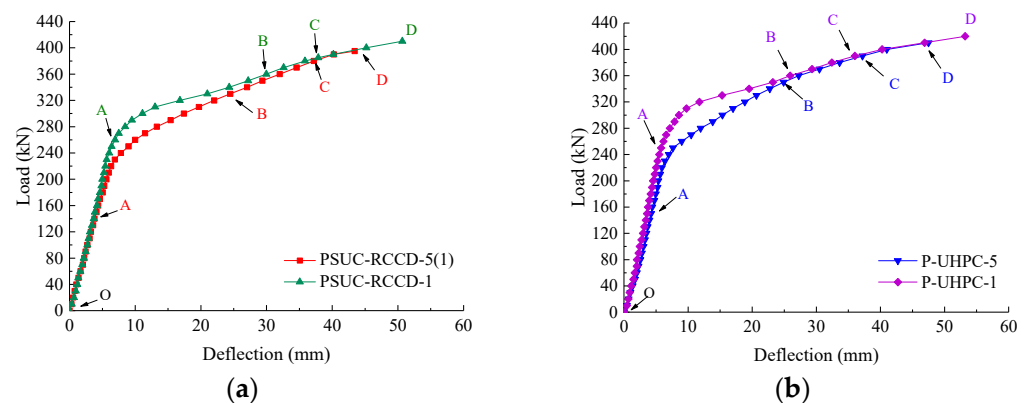


Figure 8. Comparison curves of semi-segmental and integral girders. (a) Group 1-1; (b) Group 1-2.

The curves for the specimens in the elastic phase (OA) exhibited nearly identical behavior, suggesting that the initial stiffness of semi-segmental girders closely matched that of the integral girder. The difference in the curves exists in the crack development phase I (AB), where curve AB of the integral girder is over that of the semi-segmental one, exhibiting a slow decrease in the stiffness in the integral girder, attributed to the “bridging effect” of steel fibers within it.

When the curves reached point B, the flexural crack of the specimen reached the deck slab. Following this, a convergence in the stress–strain curves for both categories of girders was noticed. This convergence occurred as the steel fibers within the cracks of the integral girder progressively lost their bond and were subsequently extracted. This phenomenon resulted in the reduction in the tensile strength of the UHPC, ultimately leading to the transformation of the cracks into dry joints.

Crack Pattern of Group 1-1 and Group 1-2

The crack pattern of PSUC-RCCD-1 and PSUC-RCCD-5(1) is shown in Figure 7a and Figure 9, respectively. Compared to these two figures, the differences between the crack patterns with different segment numbers can be discovered.

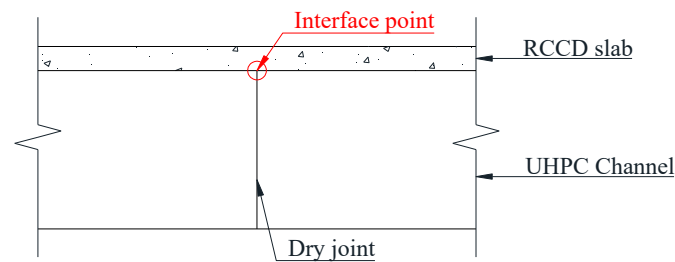


Figure 9. Schematic diagram at the interface of the channel beam and the deck slab.

The specimen was made by segments through dry-joints and the pressure of prestressing strands. As illustrated by Figure 7a, when the tension stresses on the dry-joint were larger than the pressure, the two segments were separated from each other and a crack developed along the dry-joint. On the contrary, the flexural cracks of the integral girder appeared inside the segment, which could only happen when the stress was larger than the prestressing force plus the cracking strength of the UHPC. Therefore, the cracking load of the semi-segmental girder was much lower than that of the integral girder, e.g., the cracking load of PSUC-RCCD-5(1) was 35% P_u (140 kN), while the cracking load of PSUC-RCCD-1 was 59% P_u (240 kN).

As for the horizontal cracks, they appeared earlier in the semi-segmental girder compared with the situation in the integral girder. As described in 3.1.2, a horizontal crack at the top of joint-2 took place when the load was 43% P_u (170 kN) for PSUC-RCCD-5(1), while the flexural crack was only developed to about a quarter depth of the specimen, far away from the top of the joint.

As we know, the force at the interface does not distribute uniformly because the RCCD slab was cast in one piece and the UHPC beam is disconnected at the dry-joint. As shown in Figure 9 (Intercept at Joint of PSUC-RCCD girders), due to the thin web of UHPC, this may cause shear force at the interface point of the dry-joint and the boundary between the channel beam and the deck slab, resulting in horizontal cracks starting from this interface point [28].

For PSUC-RCCD-1, the horizontal crack appeared when the load was 88% P_u (360 kN), much higher than the load in the semi-segmental girder because the horizontal crack can only be created after the flexural crack extends to the interface, as illustrated in Figure 10.

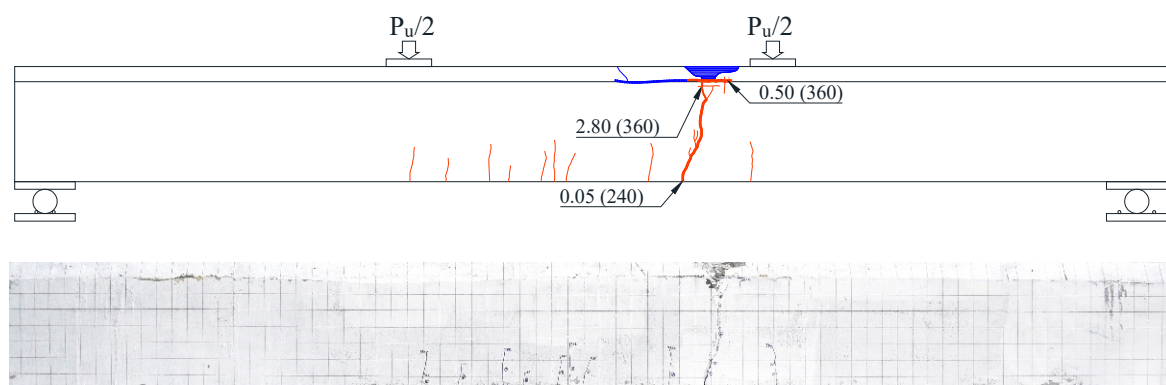


Figure 10. PSUC-RCCD-1 crack pattern at a 410 kN load.

Figure 11 shows the crack pattern of the P-UHPC specimens in Group 1-2. The difference in the cracking pattern between the semi-segmental and integral specimens is similar to that of the specimens in Group 1-1 and will not be discussed herein.

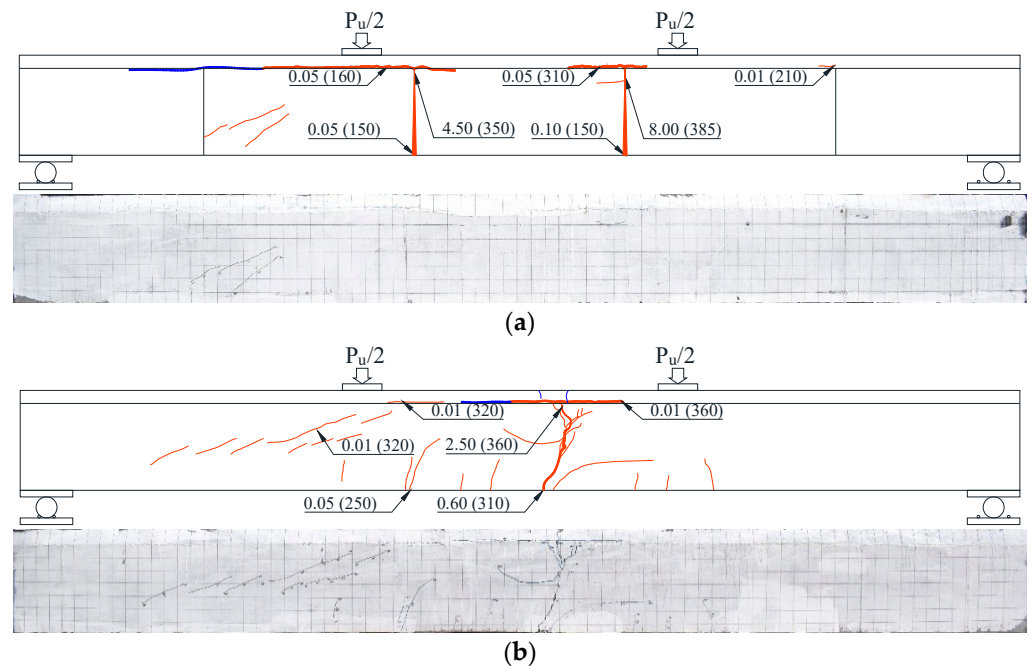


Figure 11. P-UHPC composite box girder crack pattern. (a) P-UHPC-5 crack pattern at a 410 kN load; (b) P-UHPC-1 crack pattern at a 420 kN load.

3.2.2. Deck Material

Load-Deflection Curves of Group 2-1 and Group 2-2

The deck material in the PSUC-RCCD specimen was CC with a strength of 57.0 MPa, which was replaced by UHPC with a strength of 161.5 MPa to form a P-UHPC specimen. Though the difference in concrete strength in the deck slab between the PSUC-RCCD and P-UHPC specimens is large, their load-deflection curves look similar in both Groups 2-1 and 2-2, as shown in Figure 12. In this section, only the curves of Group 2-1 are described.

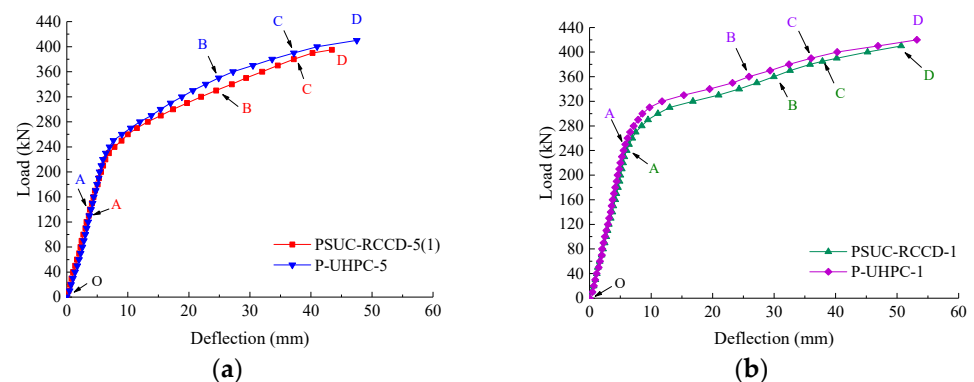


Figure 12. Comparison curves of different slabs. (a) Group 2-1; (b) Group 2-2.

In the elastic stage (OA), the curves almost overlap, which shows that the deck material strength exerts nearly no impact on the initial stiffness of the semi-segmental girders. During the crack development stage (AC), that of the specimen with the RCCD slab decreased more rapidly.

Given that the compressive strength of the RCCD slab was considerably lower than that of the UHPC slab, the specimen with the RCCD slab experienced an earlier failure (at Point D) after the prestressing strand yielded (at Point C).

However, the deck material was changed from UHPC to CC, the material strength decreased by 65%, the flexural capacity was observed to decrease by only 4%, and the maximum deflection decreased by 8%. Therefore, reducing the strength of the deck material

has no significant impact on the flexural behavior presented by the semi-segmental girders. Moreover, UHPC is prone to shrinkage cracks due to its large shrinkage strain, and quality control is difficult due to the high technique requirements, especially when it is cast in situ. Therefore, it is suitable to employ CC in the deck slab for a PSUC-deck slab composite structure.

Crack Pattern of Group 2-1 and Group 2-2

The crack pattern of Group 2-1 is shown in Figures 7a and 11a, and Group 2-2 was shown in Figures 10 and 11b. It can be found by comparison that there is no significant difference between the PSUC-RCCD and P-UHPC specimens.

As can be seen from Figure 13a, the RCCD slab was crushed in the failure phase in PSUC-RCCD-5(1), indicating that the concrete material played a complete strength role. But for P-UHPC-5, the deck slab was not totally crushed, and the compressive stress of the UHPC deck was only 129 MPa (at the top slab of joint-2), far away from its compressive strength (161 MPa). This further verifies the suggestion to use CC in the deck slab.

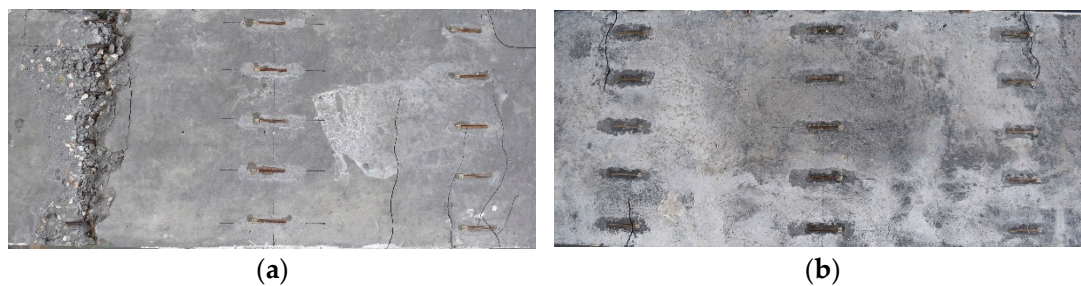


Figure 13. Deck slab of the specimen at the failure load. (a) RCCD slab of PSUC-RCCD-5(1) at 395 kN; (b) UHPC slab of P-UHPC-5 at 410 kN.

4. Calculation Methods for Cracking Moments and Flexural Capacity

4.1. For PSUC-RCCD Composite Girder

4.1.1. Cracking Moments

In the calculation of the cracking moment of the section in the PSUC-RCCD composite girder, the box section can be equated to an I-shape section, and the RCCD slab can be equated to the UHPC slab by multiplying a factor n (less than one) for the slab width, in which $n = E_{c-CC} / E_{c-UHPC}$, as shown in Figure 14.

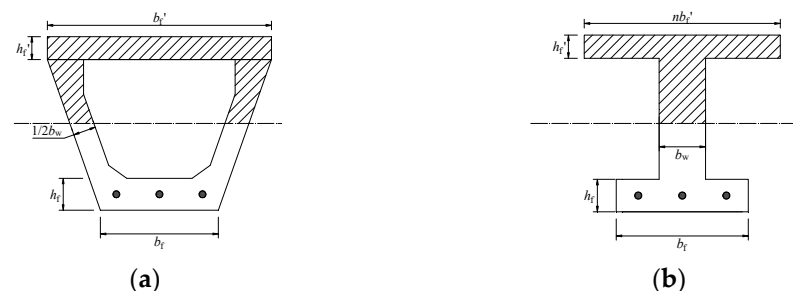


Figure 14. Equivalent cross-section for the cracking moment. (a) Cross-section; (b) Equivalent cross-section.

Dry-Joint Section

The strain and stress distribution in a dry-joint section of a semi-segmental girder is depicted in Figure 15. The crack occurs when the precompression stress (σ_p) in the section

disappears in the range of the tensile zone (y_{cr}). That is, the cracking moment (M_{cr-seg}) equals the decompression moment (M_0), as expressed in Equation (1).

$$M_{cr-seg} = M_0 = \sigma_p \cdot \frac{I_{cr}}{y_{cr}} \tag{1}$$

where M_{cr-seg} = cracking moments of the semi-segmental section; M_0 = decompression moment; σ_p = precompression stress; I_{cr} = moment of inertia of the cracking cross-section; y_{cr} = range of the tensile zone.

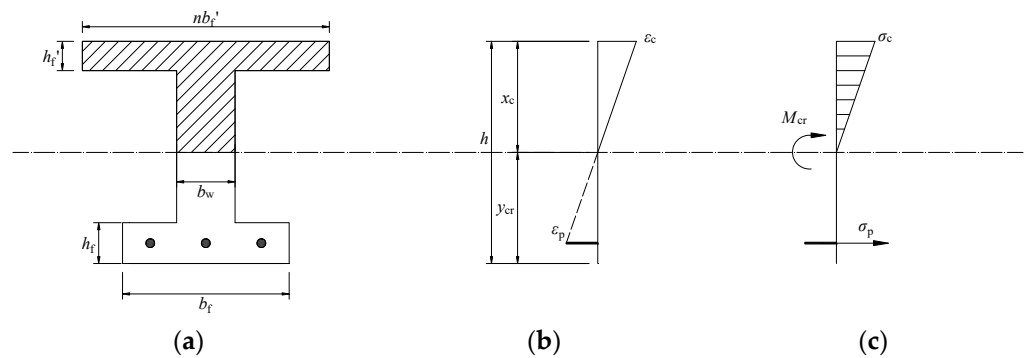


Figure 15. Strain and stress distribution in the dry-joint section at the cracking state. (a) Cross-section; (b) Strain; (c) Stress.

Integral Section

For integral sections in an integral girder or the sections among inner segments in a semi-segmental girder, the cracking moment equals the decompression moment (M_0) plus the cracking moment of the UHPC channel beam, $M_{cr-UHPC}$, as shown in Figure 16, which is expressed in Equations (2) and (3).

$$M_{cr-int} = M_0 + M_{cr-UHPC} \tag{2}$$

$$M_{cr-UHPC} = f_t \cdot (I_{cr} / y_{cr}) \tag{3}$$

where M_{cr-int} = cracking moments of the integral section; $M_{cr-UHPC}$ = cracking moment of the UHPC channel beam; f_t = tensile strength of the UHPC.

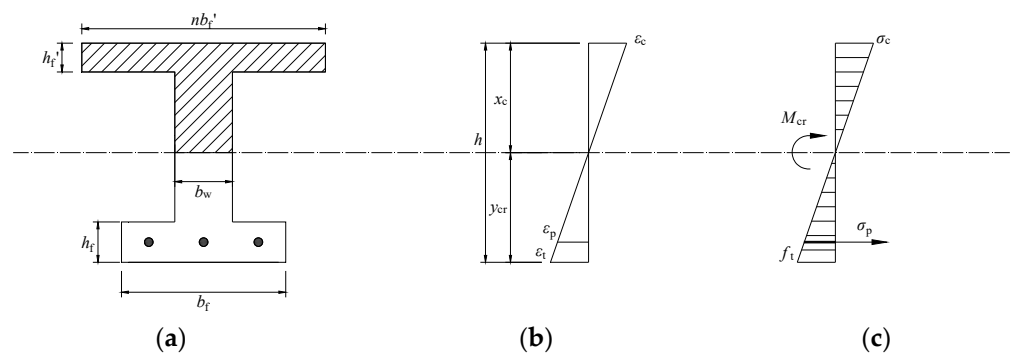


Figure 16. Strain and stress distribution in the integral section at the cracking state. (a) Cross-section; (b) Strain; (c) Stress.

4.1.2. Flexural Capacity

Dry-Joint Section

In the analysis of the flexural capacity of the PSUC-RCCD girder, the box girder can be approximated as an I-beam, as illustrated in Figure 17a. In the case of a dry-joint section,

if the neutral axis depth (x_c) is within the web when the girder reaches its failure point, the strain and stress distribution are illustrated in Figure 17b and Figure 17c, respectively.

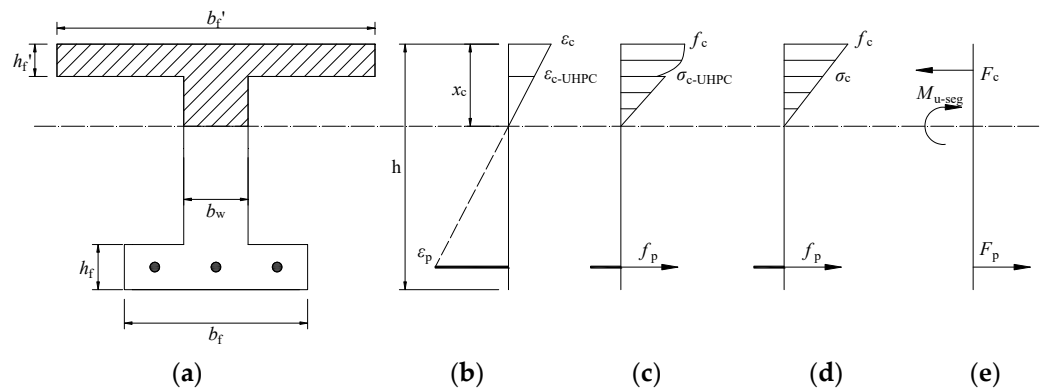


Figure 17. Diagram for the flexural capacity of the semi-segmental girder. (a) Cross-section; (b) Strains distribution; (c) Stresses distribution; (d) Simplified stress distribution; (e) Internal forces.

The compressed zone, comprising both CC and UHPC, exhibits a concrete stress distribution that can be further simplified linearly, as depicted in the following Figure 17d. This simplification is due to the similar elasticity modulus of the two materials. In this study, for instance, CC has an E_c of 38.4 GPa, and UHPC has an E_c of 44.9 GPa. Upon reaching the flexural capacity, in the compressed zone, the stress in the RCCD slab of an ideally reinforced beam is subject to crushing in the event of girder failure. This observation is supported by the results obtained from the tests conducted in this very study (as discussed in the Section Crack pattern of Group 2-1 and Group 2-2). In this scenario, the maximum concrete stress value illustrated in Figure 17d is defined as the compressive strength of the concrete, denoted as f_c .

The flexural property $M_{u,seg}$ of a dry-joint section was established by maintaining force equilibrium within the section, which is demonstrated in Figure 17e. In this representation, concentrated forces are employed to represent the compressive strains in the compression zone, while tensile forces exclusively originate from the prestressing forces.

In order to figure out the flexural capacity, it is necessary to determine the location of the neutral axis depth (x_c) first.

Assuming the x_c is within the flange section, then, an equation can be expressed as Equation (4), from which the x_c can be obtained. For an x_c less than the value of the flange depth, i.e., $x_c \leq h_f'$, it indicates the correctness of the assumption.

$$\frac{1}{2} f_c b_f' x_c = f_p A_p \tag{4}$$

where, f_c = the compressive strength of CC or UHPC; b_f' = the width of the deck slab; x_c = the neutral axis depth; f_p = the yield strength of the prestressing strand; A_p = the cross-sectional area of the prestressing strand.

Then, $M_{u,seg}$, the flexural capacity, can be correspondingly obtained using Equation (5).

$$M_{u,seg} = \frac{1}{3} f_c b_f' x_c^2 + f_p A_p (h_p - x_c) \tag{5}$$

where $M_{u,seg}$ = the flexural capacity of the semi-segmental section; b_f = the width of the UHPC bottom; h_p = the height of the prestressing strand to the top slab edge.

If the obtained x_c from Equation (4) is larger than the flange depth, i.e., $x_c > h_f'$, the neutral axis is in the web, as indicated in Figure 17. The x_c should be solved again by Equation (6)

$$\sigma_c b_f' h_f' + \frac{1}{2} (f_c - \sigma_c) b_f' h_f' + \frac{1}{2} \sigma_c b_w (x_c - h_f') = f_p A_p \tag{6}$$

where σ_c = the stress at the joint; h_f' = the height of the deck slab; b_w = the sum of web thickness.

In this case, the flexural capacity $M_{u,seg}$ can then be calculated using Equation (7)

$$M_{u,seg} = \frac{1}{3}f_c b_f' x_c^2 + f_p A_p (h_p - x_c) \quad (7)$$

Integral Section

Widely acknowledged in the field is the fact that UHPC, fortified with steel fibers at a specified volume fraction, boasts a notably high tensile strength and displays a strain-hardening behavior [25]. This observation implies the feasibility of factoring in the contribution of the tensile strength of UHPC in the case of predicting the flexural capacity of an integral section in a PSUC-RCCD girder. As elucidated in Section 3.1.1, the integral section adheres to the plane section assumption, thereby facilitating the delineation of the strain distribution within the section, as vividly illustrated in Figure 18a.

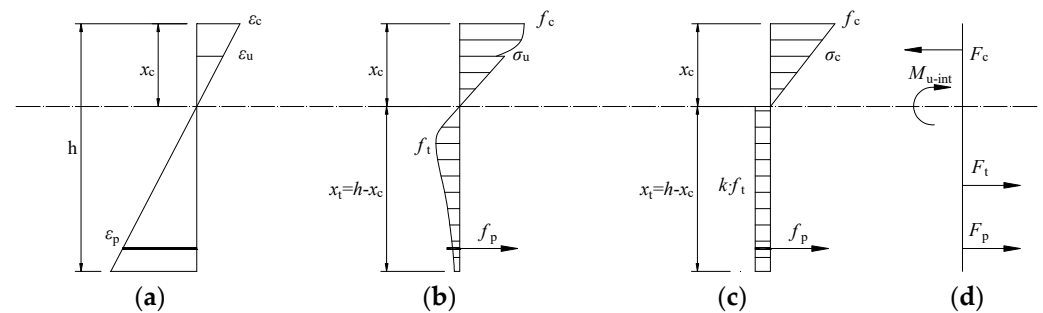


Figure 18. Diagram for the flexural capacity of the integral girder. (a) Strains distribution; (b) Stresses distribution; (c) Simplified stress distribution; (d) Internal forces.

The stresses within the section can be determined by referring to the strain distribution shown in Figure 18a and applying the stress–strain relationship for both CC and UHPC materials, as depicted in Figure 18b. The stress distribution within the concrete section is represented as a triangular shape in the compression zone and as a block in the tension zone, as illustrated in Figure 18c. It should be pointed out that the tensile stress in the tensile block in Figure 18c is $k f_t$, where k is a reduction factor to consider the real stress of UHPC. From tests, it was found that when the girder failed, the strain of the prestressing strand was 0.0052, much larger than the final tensile strain of the UHPC (0.0027), indicating that the stress of UHPC had entered into the softening branch in the stress–strain relationship curve, i.e., the stress was smaller than the tensile strength f_t and should be a multiple of a factor smaller than 1.0. The reduction factor k is taken as 0.25 by referring to the suggestion in the literature [29] through the regression analysis of the experimental data.

The determination of the flexural capacity ($M_{u,int}$) of an integral section involves the establishment of force equilibrium within the section, as depicted in Figure 18d. Analogous to the procedure employed in calculating the flexural strength of a dry-joint segment, evaluating the flexural capacity of an integral section necessitates the consideration of two scenarios regarding the location of the neutral axis.

If $x_c \leq h_f'$, the $M_{u,int}$ can be obtained using Equations (8) and (9).

$$M_{u,int} = \frac{1}{3}f_c b_f' x_c^2 + f_p A_p (h_p - x_c) + x_t b_w k f_t (h - x_c - \frac{1}{2} x_t) + k f_t (b_f - b_w) h_f (h - x_c - \frac{1}{2} h_f) \quad (8)$$

$$\frac{1}{2} f_c b_f' x_c = f_p A_p + x_t b_w k f_t + k f_t (b_f - b_w) h_f \quad (9)$$

where $M_{u,int}$ = the flexural capacity of the integral section; x_t = the height of the tension zone; k = the reduction factor of f_t ; h_f = the height of the UHPC bottom.

If $x_c > h_f'$, the $M_{u,int}$ can be obtained using Equations (10) and (11).

$$M_{u,int} = \frac{1}{3}f_c b_f' x_c^2 + f_p A_p (h_p - x_c) + k f_t b_w x_t (h - x_c - \frac{1}{2}x_t) + k f_t (b_f - b_w) h_f (h - x_c - \frac{1}{2}h_f) \quad (10)$$

$$\sigma_c b_f' h_f' + \frac{1}{2}(f_c - \sigma_c) b_f' h_f' + \frac{1}{2}\sigma_c b_w (x_c - h_f') = f_p A_p + k f_t b_w x_t + k f_t (b_f - b_w) h_f \quad (11)$$

4.2. For the P-UHPC Girder

For dry-joint or integral sections in the P-UHPC girder, the cracking moments and flexural capacity can be calculated by substituting the UHPC compression strength instead of the CC compression strength in the deck slab into Equations (1)–(11), respectively.

4.3. Verification of the Calculating Methods

4.3.1. Verification of the Calculating Methods for the Cracking Moment

For the specimens in this study, the bending moments in the sections between the two loads are constant. Consequently, the initial cracking in the semi-segmental girder is expected to occur in the dry-joint sections near the central span. The test cracking moments for these dry-joint sections can be determined from the test cracking load of the semi-segmental girder.

In the cracking moment calculation, Equation (1) is used for PSUC-RCCD-5(1), PSUC-RCCD-5(2), and P-UHPC-5, in which the x_c is located in the UHPC webs, while Equations (2) and (3) is used for PSUC-RCCD-1 and P-UHPC-1, in which the x_c is located in UHPC webs.

The calculated and test cracking moments as well as their comparisons are presented in Table 7.

Table 7. Comparison of the calculated cracking moment and test results.

Girder Notations	$M_{cr,exp}$ (kN·m)	$M_{cr,cal}$ (kN·m)	$M_{cr,cal}/M_{cr,exp}$
PSUC-RCCD-5(1)	84	83	0.99
PSUC-RCCD-5(2)	84	83	0.99
PSUC-RCCD-1	144	142	0.99
P-UHPC-5	90	84	0.93
P-UHPC-1	150	153	1.02
		Mean value	0.98
		Standard deviation	0.028

The average ratio of the calculated cracking moment to the test value is 0.98, and the standard deviation is 0.028. This suggests that the calculated value closely aligns with the test value, demonstrating a high level of agreement. Therefore, Equations (1)–(3) can be used for cracking moments in the dry-joint section and integral section, respectively.

4.3.2. Verification and Discussion of the Calculation Methods for Flexural Capacity Verification

In the case of the semi-segmental specimens employed here, it is expected that the failure will occur within the dry-joint sections located near the central span. This enables a reduction in the test flexural strength of the dry-joint segment to be deduced from the test flexural capacity of the girder.

When calculating the flexural capacity, Equation (5) is employed for the PSUC-RCCD-5(1) and PSUC-RCCD-5(2), because their x_c is located in RCCD slabs; while for the P-UHPC-5, Equation (5) is used because its x_c is located in the UHPC slab; in addition, Equations (10) and (8) are used for PSUC-RCCD-1 and P-UHPC-1, respectively, because the x_c is located in the web in the former, while it is located in the slab in the latter.

Table 8 presents the calculation results of the flexural capacity for the dry-joint and integral sections as well as the comparison results.

Table 8. Flexural capacity of the specimens.

Girder Notations	$M_{u.exp}/kN\cdot m$	$M_{u.cal}/kN\cdot m$	$M_{u.cal}/M_{u.exp}$
PSUC-RCCD-5(1)	237	209	0.88
PSUC-RCCD-5(2)	240	209	0.87
PSUC-RCCD-1	246	229	0.93
P-UHPC-5	246	215	0.87
P-UHPC-1	252	237	0.94
		Mean	0.90
		Standard deviation	0.033

The differences between the calculated flexural capacity ($M_{u.cal}$), comprising both $M_{u,seg}$ and $M_{u,int}$, and experimental values ($M_{u.exp}$) for all specimens consistently fall within a 15% margin of error. The mean ratio of calculated to experimental values across all specimens is 0.90, with a standard deviation of less than 0.05. This indicates that the approach employed for determining the flexural capacity of these derived specimens exhibits a commendable level of accuracy, making it a reliable approach for calculating PSUC-RCCD and P-UHPC girders.

Discussion

In accordance with the guidelines outlined in codes [30,31], the calculation of flexural capacity in a semi-segmental girder comprises multiplying a resistance factor (φ) by the intrinsic flexural capacity of the corresponding integral girder, as detailed in Equation (12). It is important to highlight that, particularly for semi-segmental girders incorporating unbonded prestressing strands, a distinct resistance factor (φ) is stipulated and is specifically set at the value of 0.85.

$$M_{u,\varphi} = \varphi M_{u,int} \quad (12)$$

where $M_{u,\varphi}$ = cracking moments of a semi-segmental section calculated by the resistance factor; φ = the resistance factor.

The ultimate test resistance factor (φ) can be determined by means of dividing the flexural capacities of the semi-segmental girders by those of the corresponding integral girders. The results are outlined in Table 9, with values ranging from 0.96 to 0.98. These values indicate an average of 0.98, which is in proximity to 1.0 and is significantly different from the prescribed value of 0.85.

Table 9. Flexural capacity comparison between semi-segmental and integral girders.

Comparison Girders	$M_{exp,seg}/M_{exp,int}$
PSUC-RCCD-5(1)/PSUC-RCCD-1	0.96
PSUC-RCCD-5(2)/PSUC-RCCD-1	0.98
P-UHPC-5/P-UHPC-1	0.98
Mean value	0.98

It is crucial to emphasize that the semi-segmental girders described in this paper are not exclusively composed of individual segments. Instead, the deck slabs are cast in place to create a monolithic slab, giving rise to a configuration that can be characterized as semi-segmental or semi-integral girders. This design offers improved structural integrity and yields a higher-level flexural capacity compared to typical semi-segmental girders. This represents a notable advantage of this particular girder configuration. It is obvious that the resistance factor is different for such a type of girder compared to the common

segmental girder. In the initial design phase, the flexural strength of the dry-joint segment can be calculated by multiplying the 0.95 resistance factor by that of the integral section in reverse.

5. Conclusions

This paper presents a study regarding the flexural performance of PSUC-RCCD composite girders. The influence of the segment number and deck material on the behavior of the PSUC-RCCD composite girder was investigated. The obtained outcomes can be listed as follows:

- (1) All five specimens behaved similarly, no matter whether the channel beams were segmental or integral or whether the deck slabs were CC or UHPC materials. The entire loading process can be classified into the elastic phase, the cracks development phase, and the failure phase. The segment number and the concrete material property of the deck slab have no significant impact on the flexural behavior of the composite girders, indicating that the PSUC-RCCD composite girders can be used in bridge superstructures.
- (2) The dry-joint in the PSUC-RCCD girders does not greatly reduce the flexural capacity of the section, but it does significantly decrease the cracking capacity. The test results indicate that the flexural capacity of semi-segmental girders is 0.96~0.98 times that of the integral girders, but the semi-segmental girders (section) are much lower than those of integral girders (section); the former is only 0.58~0.60 of the latter. This is because of the “bridging effect” of the steel fibers in the integral girders, which makes the specimens crack later, but for the ultimate capacity, the contribution of the tensile stresses in the UHPC is limited because the steel fibers are constantly being pulled out. Therefore, the low cracking moment at the dry-joint section should be paid attention to in practice. To add epoxy to the dry-joints may improve the cracking moment, but the durability of the prestressing strands in them should still be carefully considered in the design.
- (3) For both semi-segmental and integral girders, reducing the strength of the deck slab by changing the material from UHPC to CC does not significantly affect their flexural behaviors. Their load-deflection curves are almost overlapped. The cracking moments as well as the flexural capacity of the specimens with a UHPC deck are 1.04~1.15 and 1.02~1.04 times those in the specimens with a CC deck, which means the UHPC material in the deck slab could not be fully utilized, and it is suitable to employ CC in the deck slab to form a PSUC-RCCD to achieve a structurally efficient and economical solution.
- (4) Based on the findings of the present experimental study, calculation methods for the cracking moments and flexural capacity of semi-segmental and integral sections in PSUC-RCCD and P-UHPC girders have hereby been developed. These calculated results align perfectly with the test findings. The present discussion further suggests that the recommended resistance factor of 0.85 in certain design codes underestimates the flexural capacity of the semi-segmental girders in this paper, as they are not entirely composed of segments but are semi-segmental in nature. In the initial design phase, one can estimate the flexural strength of the dry-joint segment by calculating it as 0.95 times that of the integral section’s capacity using a resistance factor in reverse.

Author Contributions: Conceptualization, B.C., J.S. and C.N.; methodology, B.C. and Y.C.; validation, J.Z. and J.S.; investigation, Y.C.; data curation, Y.C. and J.Z.; writing—original draft preparation, Y.C.; writing—review and editing, B.C., J.Z. and C.N.; supervision, B.C., J.Z., J.S. and C.N.; funding acquisition, B.C. All authors have read and agreed to the published version of the manuscript.

Funding: This research was funded by the National Key R&D Program of China (2018YFC0705400).

Data Availability Statement: Data are contained within the article.

Conflicts of Interest: The authors declare no conflict of interest.

References

1. Mishra, O.; Singh, S.P. An overview of microstructural and material properties of ultra-high-performance concrete. *J. Sustain. Cem. Mater.* **2019**, *8*, 97–143. [[CrossRef](#)]
2. Mishra, S.; Mistry, R. Reviewing some properties of ultra high performance concrete. *Int. J. Eng. Res. Technol.* **2020**, *6*, 108–121. [[CrossRef](#)]
3. Larsen, I.L.; Thorstensen, R.T. The influence of steel fibres on compressive and tensile strength of ultra high performance concrete: A review. *Constr. Build. Mater.* **2020**, *256*, 119459. [[CrossRef](#)]
4. Sharma, R.; Jang, J.G.; Bansal, P.P. A comprehensive review on effects of mineral admixtures and fibers on engineering properties of ultra-high-performance concrete. *J. Build. Eng.* **2022**, *45*, 103314. [[CrossRef](#)]
5. Mostafa, S.A.; Faried, A.S.; Farghali, A.A.; EL-Deeb, M.M.; Tawfik, T.A.; Majer, S.; Abd Elrahman, M. Influence of Nanoparticles from Waste Materials on Mechanical Properties, Durability and Microstructure of UHPC. *Materials* **2020**, *13*, 4530. [[CrossRef](#)] [[PubMed](#)]
6. Zhou, M.; Lu, W.; Song, J.; Lee, G.C. Application of Ultra-High Performance Concrete in bridge engineering. *Constr. Build. Mater.* **2018**, *186*, 1256–1267. [[CrossRef](#)]
7. Graybeal, B.A.; Brühwiler, E.; Kim, B.S.; Toutlemonde, F. International Perspective on UHPC in Bridge Engineering. *J. Bridge Eng.* **2020**, *25*, 04020094. [[CrossRef](#)]
8. Rahman, M.; McQuaker, T. Application of Ultra-High Performance Concrete in Bridge Engineering in China. In Proceedings of the First International Interactive Symposium on UHPC 2016, Des Moines, IA, USA, 18–20 July 2016; pp. 1–8. [[CrossRef](#)]
9. Zheng, W.; Lv, X. Literature review of reactive powder concrete. *J. Build. Struct.* **2015**, *36*, 44–58. (In Chinese) [[CrossRef](#)]
10. Yan, P.Y. Application of UHPC in China. In Proceedings of the 1st International Symposium of ACF on Ultra High Performance Concrete, Kolkata, India, 7 October 2015; pp. 79–82.
11. Shuping, G. Application of RPC in Railway prestressed prefabricated bridge. *Ready-Mix. Concr.* **2007**, *3*, 19–21.
12. Shao, X.; Yi, D.; Huang, Z.; Zhao, H.; Chen, B.; Liu, M. Basic Performance of the Composite Deck System Composed of Orthotropic Steel Deck and Ultrathin RPC Layer. *J. Bridge Eng.* **2013**, *18*, 417–428. [[CrossRef](#)]
13. Su, J.; Ma, X.; Chen, B.; Sennah, K. Full-scale bending test and parametric study on a 30-m span prestressed ultra-high performance concrete box girder. *Adv. Struct. Eng.* **2020**, *23*, 1276–1289. [[CrossRef](#)]
14. Chen, B.C.; Huang, Q.W.; Wang, Y.Y.; Guo, B.; Luo, X.; Jiang, S.H. Design and construction of the first Ultra-high Performance Concrete (UHPC) arch bridge in China. *J. China Foreign Highw.* **2016**, *36*, 67–71. (In Chinese) [[CrossRef](#)]
15. Wang, Y.; Shao, X.; Cao, J. Experimental Study on Basic Performances of Reinforced UHPC Bridge Deck with Coarse Aggregates. *J. Bridge Eng.* **2019**, *24*, 04019119. [[CrossRef](#)]
16. Voo, Y.L.; Foster, S.J.; Voo, C.C. Ultrahigh-performance concrete segmental bridge technology: Toward sustainable bridge construction. *J. Bridge Eng.* **2015**, *20*, B5014001. [[CrossRef](#)]
17. Voo, Y.L.; Hafezolghorani, M.; Foster, S.J. Application of Ultra—High Performance Fiber Reinforced Concrete Technology for Present and Future. In Proceedings of the 2nd International Conference on UHPC Materials and Structures, Fuzhou, China, 7–10 November 2018; pp. 6–20.
18. Dadmand, B.; Pourbaba, M.; Sadaghian, H.; Mirmiran, A. Effectiveness of steel fibers in ultra-high-performance fiber-reinforced concrete construction. *Adv. Concr. Constr.* **2020**, *10*, 195–209. [[CrossRef](#)]
19. Makhbal, T.O.; Han, S.M.; Kim, D.O. Flexural behavior of ultra high performance fiber reinforced concrete 50 m composite box girder. In Proceedings of the 2nd International Conference on UHPC Materials and Structures, Fuzhou, China, 7–10 November 2018; pp. 777–790.
20. Lee, S.J.; Makhbal, T.O.; Kim, S.T.; Han, S.M. Flexural Behavior of Segmental U-Girder and Composite U-Girder Using Ultra High Performance Concrete. *J. Korean Recycl. Constr. Resour. Inst.* **2017**, *5*, 290–297. [[CrossRef](#)]
21. Chen, Y.C.; Zhou, J.L.; Guo, F.Z.; Chen, B.C.; Nuti, C. Experimental Study on the Flexural Behaviors of Prestressed Segmental Ultra—High—Performance Concrete Channels and Reinforced Conventional Concrete Deck Composite Girders. *Buildings* **2023**, *13*, 1841. [[CrossRef](#)]
22. Buyukozturk, O.; Bakhom, M.M.; Michael Beattie, S. Shear behavior of joints in precast concrete segmental bridges. *J. Struct. Eng.* **1990**, *116*, 3380–3401. [[CrossRef](#)]
23. Ahmed, G.H.; Aziz, O.Q. Stresses, deformations and damages of various joints in precast concrete segmental box girder bridges subjected to direct shear loading. *Aziz. Eng. Struct.* **2020**, *206*, 110151. [[CrossRef](#)]
24. GB/T 31387-2015; Reactive Powder Concrete. Standards Press of China: Beijing, China, 2015. (In Chinese)
25. SIA 2052:201X; Construction, Recommendation: Ultra-High Performance Fiber Reinforced Cement-Based Composites (UHPFRC). EPFL-Swiss Federal Institute of Technology: Lausanne, Switzerland, 2016.
26. 50081-2002; Standard for Method of Mechanical Properties on Ordinary Concrete. Standards Press of China: Beijing, China, 2002. (In Chinese)
27. GB/T 228.1-2010; Metallic Materials—Tensile Testing—Part 1: Method of Test at Room Temperature. Standards Press of China: Beijing, China, 2010. (In Chinese)
28. Herrera, A.; Baby, F.; Marchand, P.; Toutlemonde, F. UHPFRC direct shear characterization applied to web-flange shear design of T-Shaped Girders. In Proceedings of the AFGC-ACI-Fib-RILEM Int. Symposium on Ultra-High Performance Fibre-Reinforced Concrete (UHPFRC 2017), Montpellier, France, 2–4 October 2017; pp. 431–440.

29. Li, L. Mechanical Behavior and Design Method for Reactive Powder Concrete Beams. Ph.D. Thesis, College of Civil Engineering, Harbin Institute of Technology, Harbin, China, 2010. (In Chinese)
30. *LRFDUS-6*; AASHTO LRFD Bridge Design Specifications. American Association of State Highway and Transportation Officials: Washington, DC, USA, 2012.
31. *DBJ 43/T 325-2017*; Technical Specification for Reactive Powder Concrete Structures. China Architecture & Building Press: Beijing, China, 2017. (In Chinese)

Disclaimer/Publisher's Note: The statements, opinions and data contained in all publications are solely those of the individual author(s) and contributor(s) and not of MDPI and/or the editor(s). MDPI and/or the editor(s) disclaim responsibility for any injury to people or property resulting from any ideas, methods, instructions or products referred to in the content.